Science Advances
AAAS

Supplementary Materials for

Spatiotemporal gating of Stat nuclear influx by *Drosophila* Npas4 in collective cell migration

Jhen-Wei Wu *et al.*

Corresponding author: Yu-Chiuan Chang, ycc@mail.nsysu.edu.tw; Anna C.-C. Jang, ccjang@ncku.edu.tw

Sci. Adv. **8**, eabm2411 (2022)
DOI: 10.1126/sciadv.abm2411

This PDF file includes:

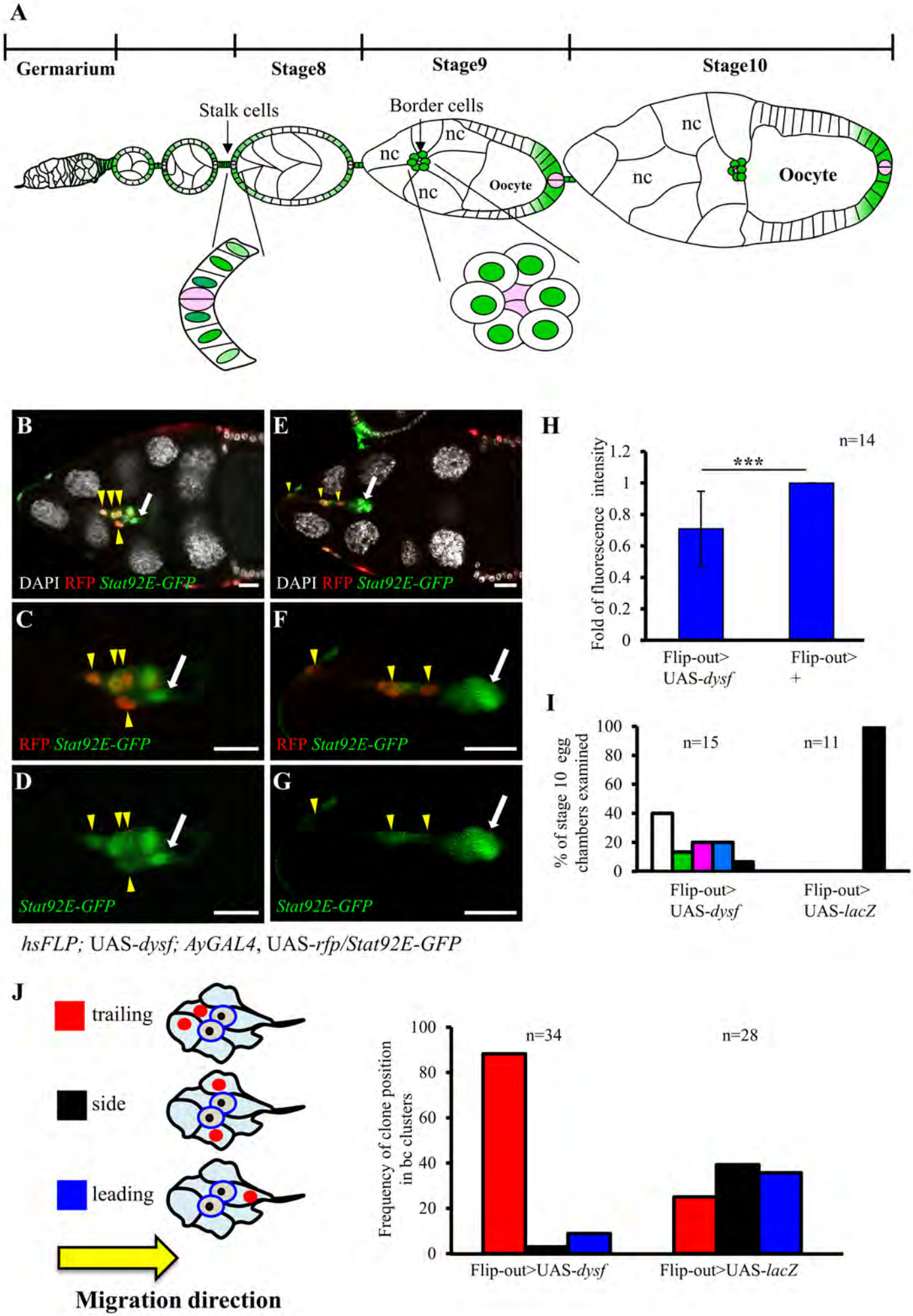
A
Germarium
Stage8
Stage9
Stage10
Stalk cells
Border cells
nc
nc
nc
Oocyte
nc
nc
Oocyte
B
DAPI RFP Stat92E-GFP
E
DAPI RFP Stat92E-GFP
C
RFP Stat92E-GFP
F
RFP Stat92E-GFP
D
Stat92E-GFP
G
Stat92E-GFP
H
n=14
***
Fold of fluorescence intensity
1.2
1
0.8
0.6
0.4
0.2
0
Flip-out>
UAS-dysf
Flip-out>
+
I
% of stage 10 egg chambers examined
100
80
60
40
20
0
n=15
n=11
Flip-out>
UAS-dysf
Flip-out>
UAS-lacZ
hsFLP; UAS-dysf; AyGAL4, UAS-rfp/Stat92E-GFP
J
trailing
side
leading
Migration direction
Frequency of clone position in bc clusters
100
80
60
40
20
0
n=34
n=28
Flip-out>UAS-dysf
Flip-out>UAS-lacZ

Fig. S1: Overexpression of Dysf suppresses cell motility and *Stat92E-GFP* expression in individual border cells. (**A**) Schematic of a *Drosophila* ovariole comprising successively developed egg chambers, each of which contains 16 germ cells covered by the follicular epithelium. *Stat92E-GFP* (green) is detected in follicle cells, including germarial precursors, stalk cells, border cells and egg chamber terminals. Border cells surround the anterior pair of polar cells (pink) to form a cluster that migrates through nurse cells (nc) and reaches the oocyte border at stage 10. (**B** to **G**) Clonal induction of *dysf* by the Flip-Out system resulted in *Stat92E-GFP* downregulation. Enlargements of the border cells are shown in C, D, F and G. DAPI (white) marked the nuclei of all follicle and germ cells. (**H**) Quantification of the ratio of fluorescence signal intensity for *Stat92E-GFP* in wild type (white arrows) and *dysf*-expressing border cells (RFP-positive; yellow arrowheads). Migrating border cells that detached from the anterior epithelia but did not reach the oocyte were used for experimentation. Values were defined as fold-change relative to the wild type. (**I**) Quantification of migration defects in border cell clusters containing *dysf*-expressing cells. (**J**) Frequency of the Flip-Out clone position in migrating border cell clusters. Definition of border cell distribution within the cluster is illustrated in the left schematic. Error bars indicate SD. n means the inspected sample size; ***P<0.001, two-tailed t test. Scale bar: 20 μm.

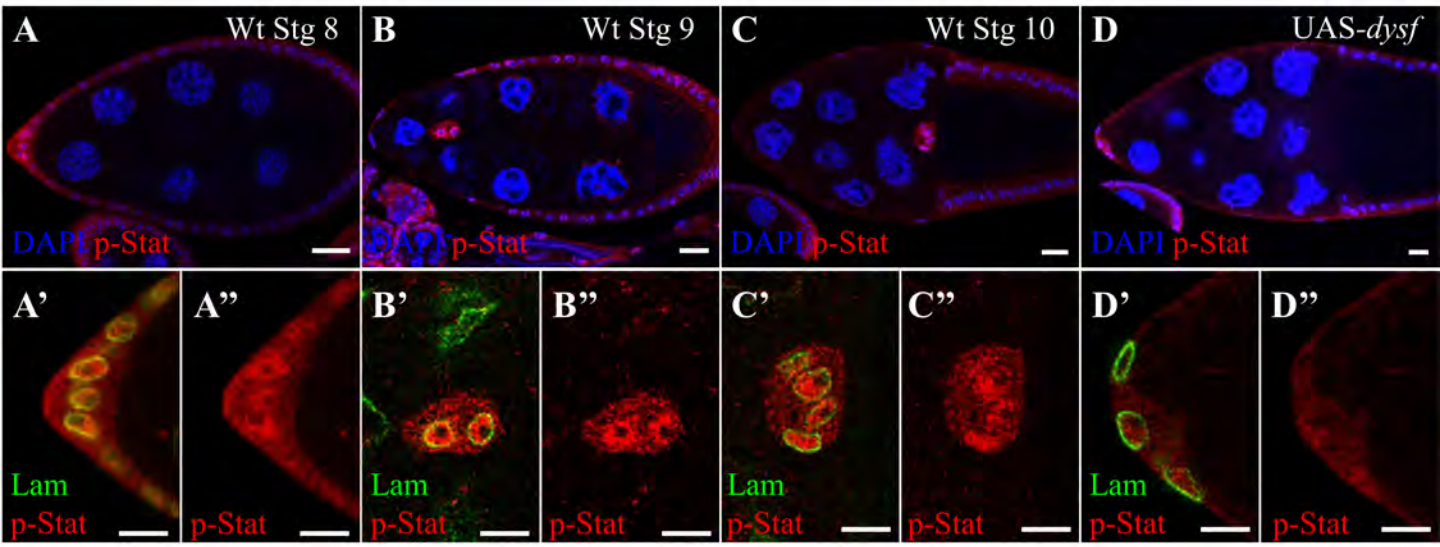
A
Wt Stg 8
DAPI p-Stat
B
Wt Stg 9
DAPI p-Stat
C
Wt Stg 10
DAPI p-Stat
D
UAS-dysf
DAPI p-Stat

A'
A"
B'
B"
C'
C"
D'
D"
Lam
p-Stat

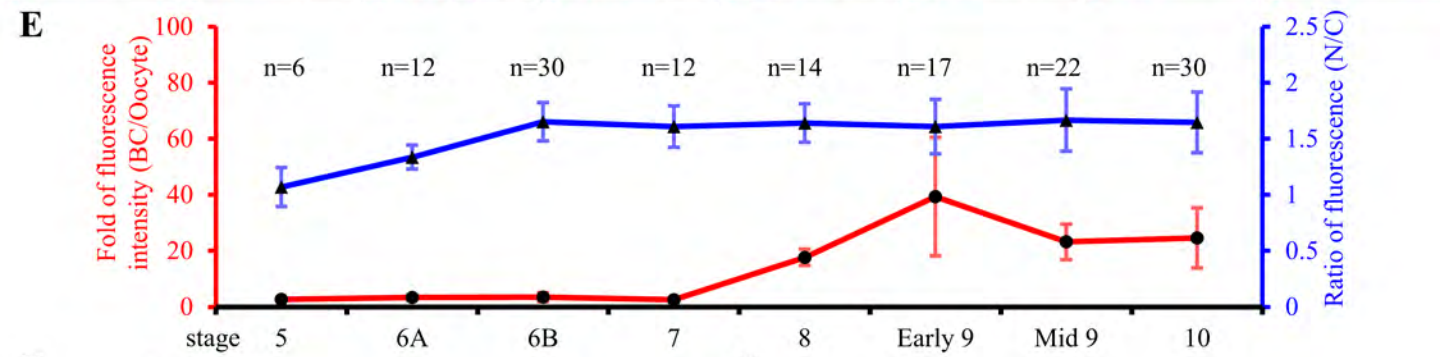
E
Fold of fluorescence intensity (BC/Oocyte)
Ratio of fluorescence (N/C)
n=6
n=12
n=30
n=12
n=14
n=17
n=22
n=30
stage 5
6A
6B
7
8
Early 9
Mid 9
10

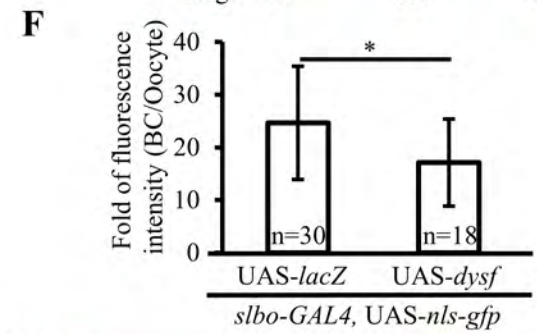
F
Fold of fluorescence intensity (BC/Oocyte)
*
n=30
n=18
UAS-lacZ
UAS-dysf
slbo-GAL4, UAS-nls-gfp

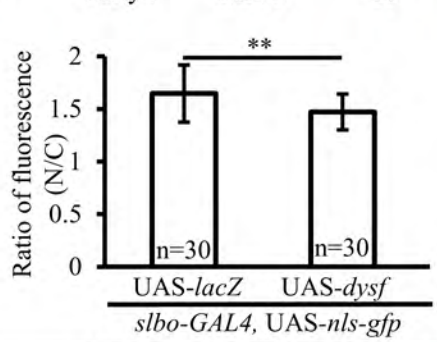
G
Ratio of fluorescence (N/C)
**
n=30
n=30
UAS-lacZ
UAS-dysf
slbo-GAL4, UAS-nls-gfp

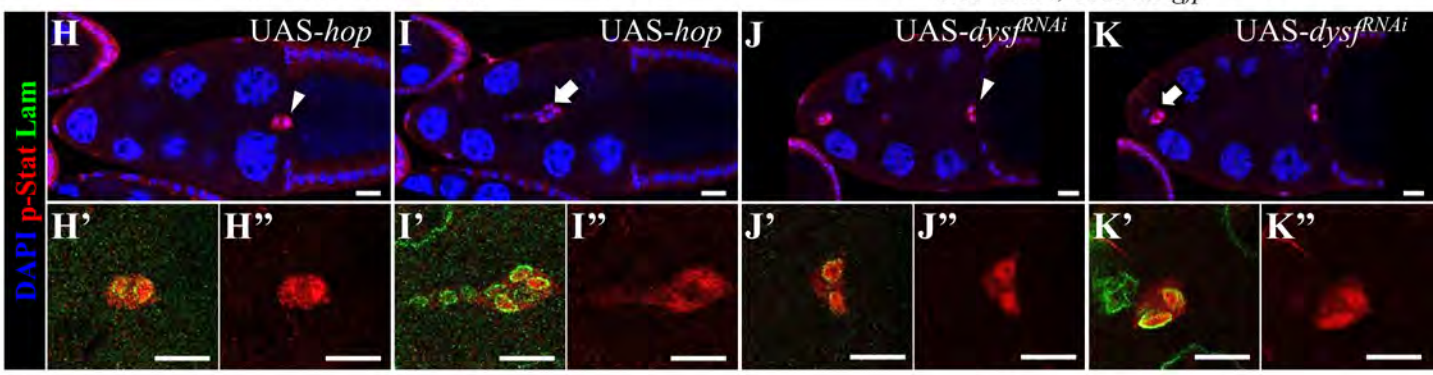
H
UAS-hop
I
UAS-hop
J
UAS-dysfRNAi
K
UAS-dysfRNAi
DAPI p-Stat Lam
H'
H"
I'
I"
J'
J"
K'
K"

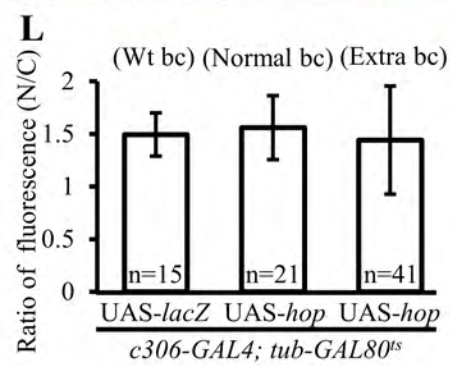
L
(Wt bc) (Normal bc) (Extra bc)
Ratio of fluorescence (N/C)
n=15
n=21
n=41
UAS-lacZ
UAS-hop
UAS-hop
c306-GAL4; tub-GAL80ts

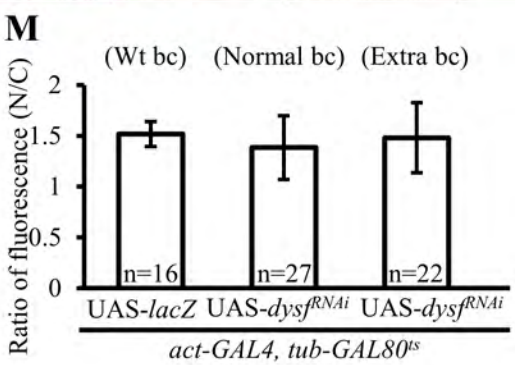
M
(Wt bc)
(Normal bc)
(Extra bc)
Ratio of fluorescence (N/C)
n=16
n=27
n=22
UAS-lacZ
UAS-dysfRNAi
UAS-dysfRNAi
act-GAL4, tub-GAL80ts

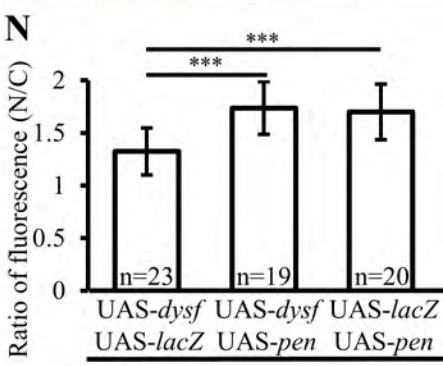
N
***
***
Ratio of fluorescence (N/C)
n=23
n=19
n=20
UAS-dysf
UAS-lacZ
UAS-dysf
UAS-pen
UAS-lacZ
UAS-pen
slbo-GAL4, UAS-nls-gfp;
tub-GAL80ts

Fig. S2: Dysf upregulation impairs the expression and nuclear transport of p-Stat in border cells. (**A** to **D**) Confocal micrographs of egg chambers stained for p-Stat (red) and DAPI (blue). Anterior follicle cells and border cells are magnified in lower panels to display p-Stat distribution in nuclei labeled by Lamin staining (green). (**E**) Quantitative analyses of p-Stat expression in *Drosophila* oogenesis. Fold change of p-Stat staining was determined by the fluorescence intensity of anterior follicle cells (stage 5 to 8) or border cells (stage 9 to 10) divided by that of the oocyte (red plot). The nuclear transport level of p-Stat was measured by its ratio of nucleus-cytoplasm (N/C) staining, a value of the nuclear signal normalized with the cytoplasm in the same cell (blue plot). (**E** and **F**) Quantitation results of the fold change of p-Stat staining. (**G** and **L** to **N**) Quantitation results of the N/C ratio of p-Stat staining. (**H** to **K**) Different focal planes of micrographs taken from the same egg chambers display display extra recruited border cells (Extra bc; arrows) and normally migrating border cell clusters (Normal bc; arrowheads) in the indicated genotype. (**N**) Co-expression of *pen* restored the reduction of p-Stat N/C ratio by *dysf*. Unless otherwise indicated, experiments were conducted with stage-10 egg chambers. n represents the number of border cells examined; *$p < 0.05$, **$p < 0.01$, ***$p < 0.001$, two-tailed t test. Error bars indicate SD. Scale bar: 20 μm (A to D and H to K) and 10 μm (A'-A'' to D'-D'' and H'-H'' to K'-K'').

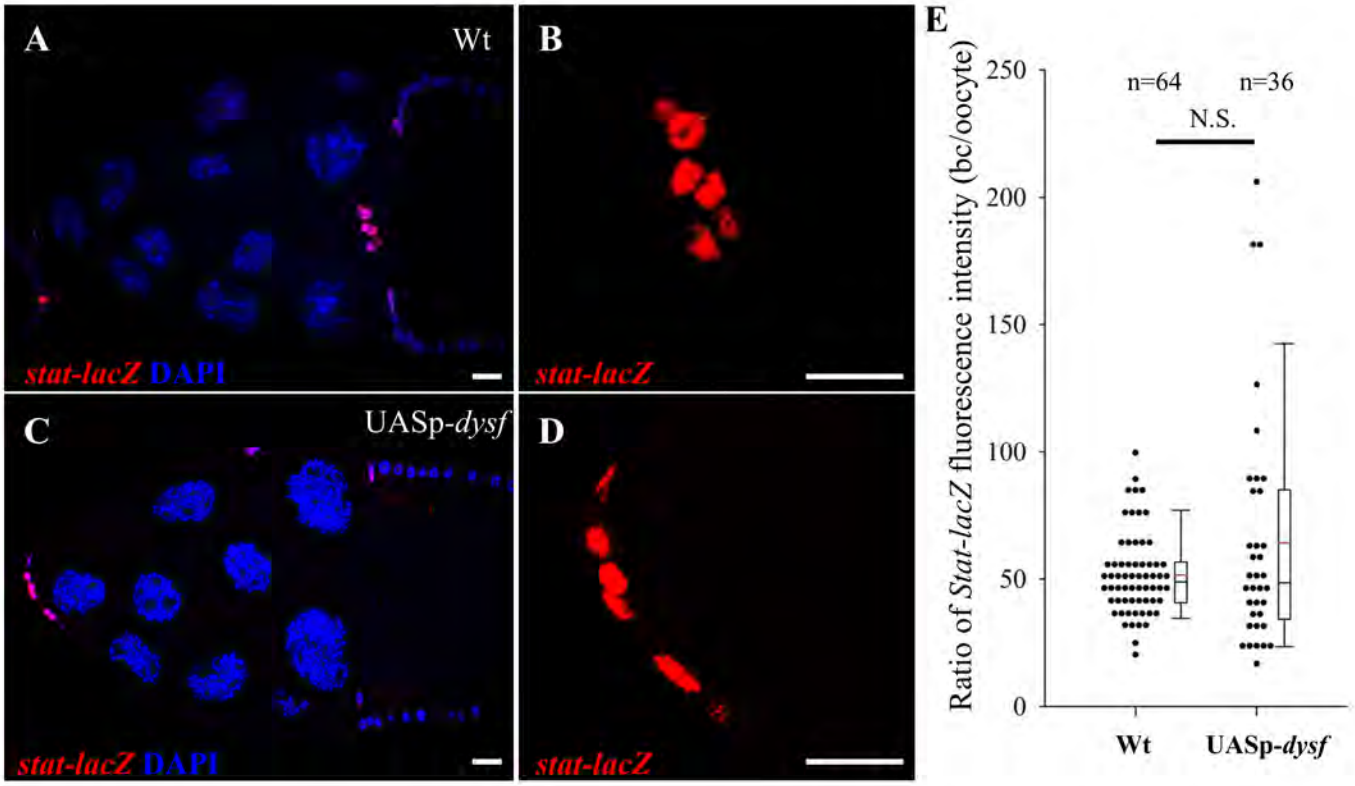

Fig. S3: Dysf overexpression does not suppress transcriptional expression of the *stat* gene. The *stat-lacZ* reporter was used to analyze transcriptional expression of *stat* in stage 10 egg chambers. (**A** to **D**) Anti-β-galactosidase staining (red) shows the expression pattern of *stat-lacZ* in stage 10 egg chambers of the indicated genotypes. DAPI (blue) stains nuclear DNA to mark nuclei. (**E**) Quantification of *stat-lacZ* expression in the indicated genotypes. Values are defined by the fold-change of fluorescence signal intensity of border cells over that of the internal control (oocyte). The box plot shows medians (black lines), and means (red lines), the 25th and 75th range (boxes), and the 5th and 95th percentiles (whiskers). N.S. stands for Not Significant. n represents the number of border cells examined and analyzed by two-tailed t test. Scale bars: 20 μm.

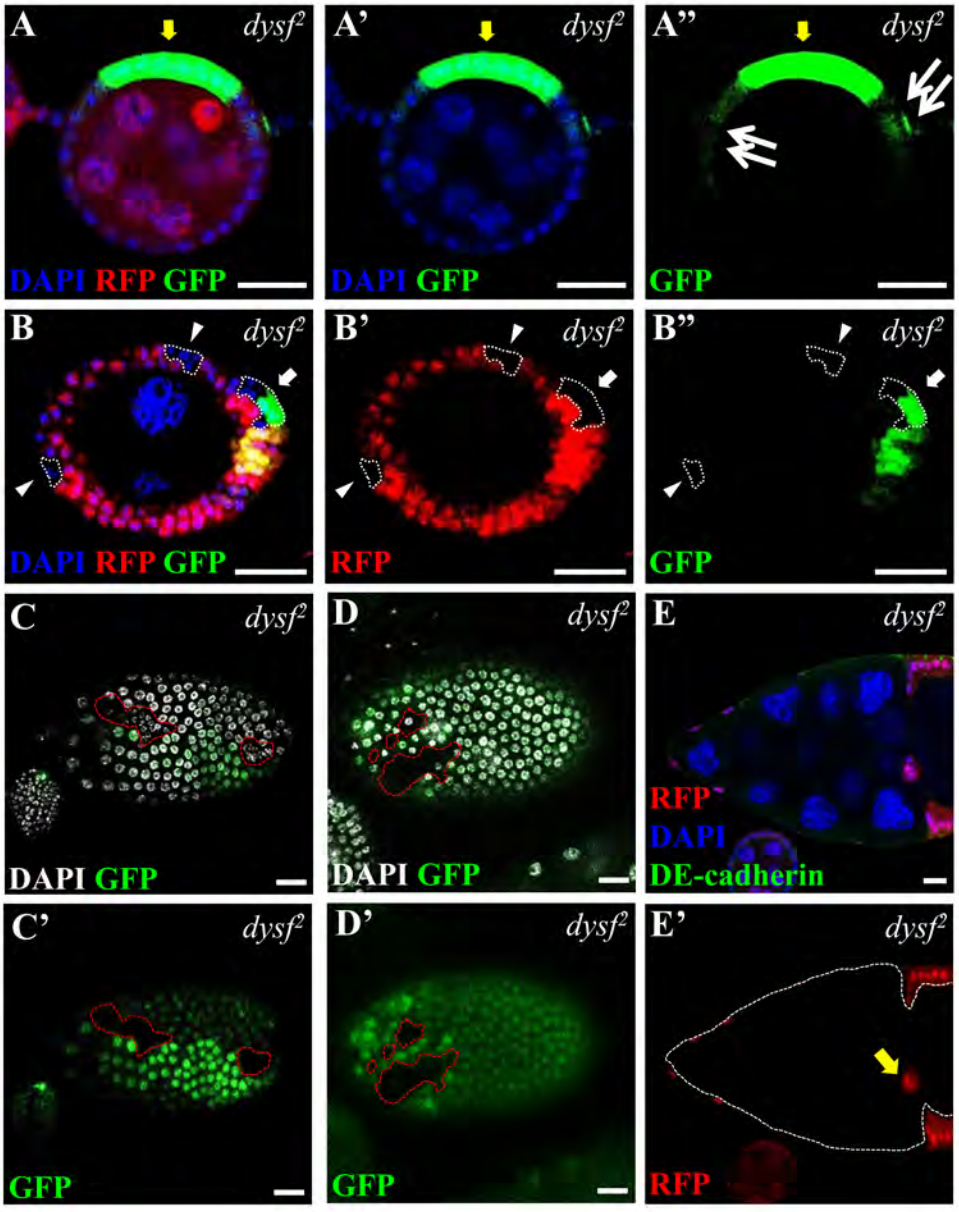
A
dysf²
DAPI RFP GFP
A'
dysf²
DAPI GFP
A"
dysf²
GFP
B
dysf²
DAPI RFP GFP
B'
dysf²
RFP
B"
dysf²
GFP
C
dysf²
DAPI GFP
D
dysf²
DAPI GFP
E
dysf²
RFP
DAPI
DE-cadherin
C'
dysf²
GFP
D'
dysf²
GFP
E'
dysf²
RFP

Fig. S4: Characterization of *dysf²* mutation effect on follicular development. Confocal micrographs of egg chambers carrying *dysf²*-homozygous mutation. DAPI staining marks nuclei (blue in A, B and E; white in C and D). (**A** and **B**) *dysf²* mutant clones labeled by the absence of RFP (red) shows ectopic expression of *Stat92E-GFP* (green, yellow arrows). (**A**) Background enhancement of Figure 3D-E exposed the relatively-low endogenous expression of *Stat92E-GFP* in the terminal regions of egg chambers (double arrows), compared to the ectopic expression (yellow arrows) in *dysf²* mutant clones. (**B**) A 3D reconstruction from 5 consecutive images exhibits ectopic expression of *Stat92E-GFP* with incomplete penetrance by *dysf²* mutation in follicles (RFG-negative; dotted circles); some mutant cells did not express this reporter (arrowheads). In some cases, cells originated from the same clone did not ectopically express Stat92E-GFP simultaneously (white arrows). (**C** and **D**) *dysf²* mutant cells, outlined and labeled by the absence of GFP (green), display morphological defects in follicle epithelia. (**E**) A stage 10 egg chamber with *dysf²* germline mutation (RFP-negative and outlined) displays normal border cell migration (white arrow). Scale bars: 20 μm.

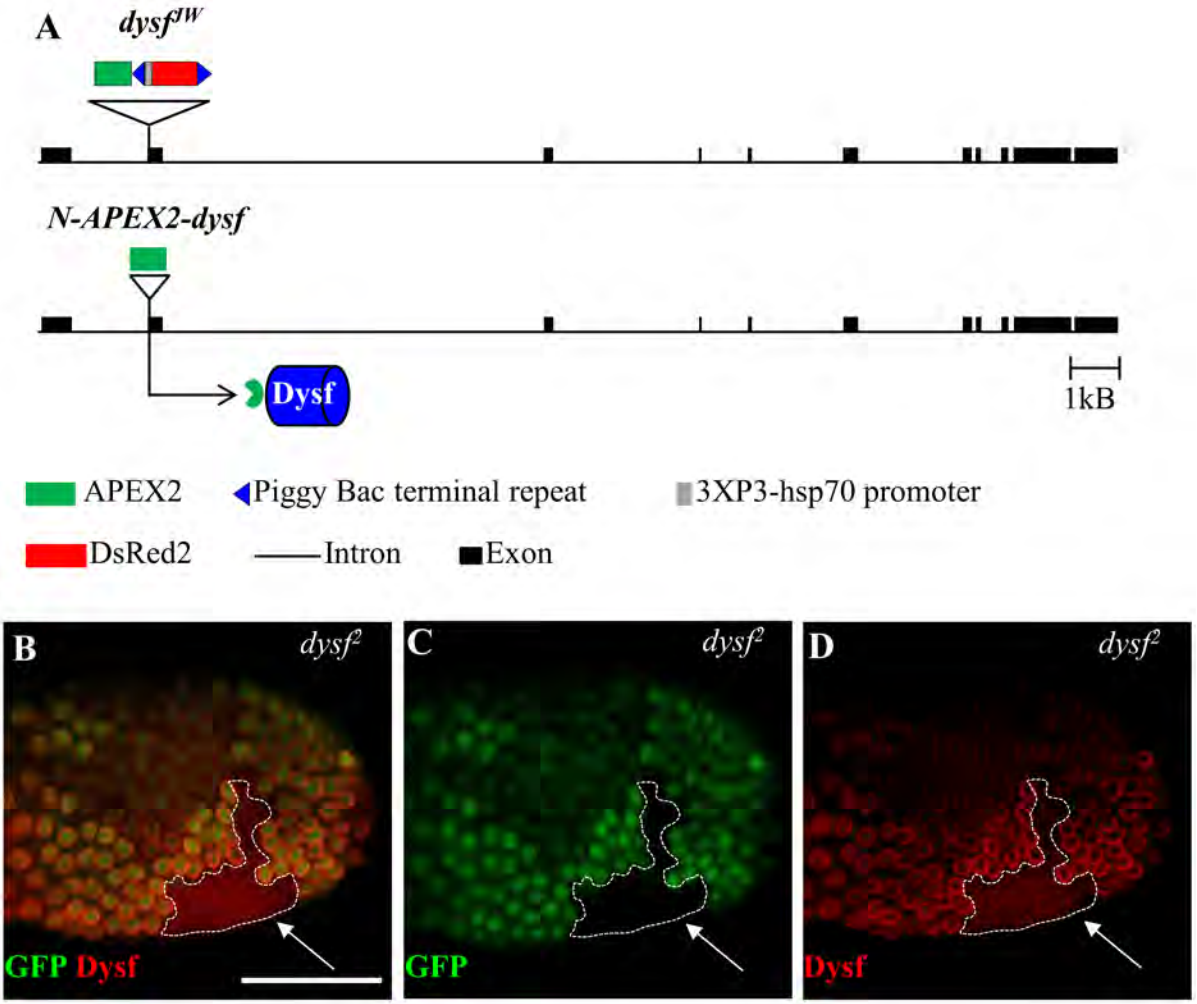

Fig. S5: Construction of novel *dysf* alleles and examination for the specificity of anti-Dysf antibody. (**A**) A molecular map of the *dysf* locus and the domain structure of the inserted DNA fragment, *dysf*^{JW} (see material and methods). The *dysf*^{JW} insertion inhibits synthesis of full-length Dysf, leading to lethal mutation. *N-APEX2-dysf* encodes APEX2 fused to the N-terminal of Dysf and was employed for proximity labeling. (**B-D**) Micrographs of egg chambers display *dysf*^{2}-homozygous mutant cells (GFP-negative, dotted circles) stained with anti-Dysf antibody. Loss of the nuclear membrane staining in *dysf*^{2}-mutant clones confirmed the specificity of anti-Dysf antibody. Scale bars: 20 μm.

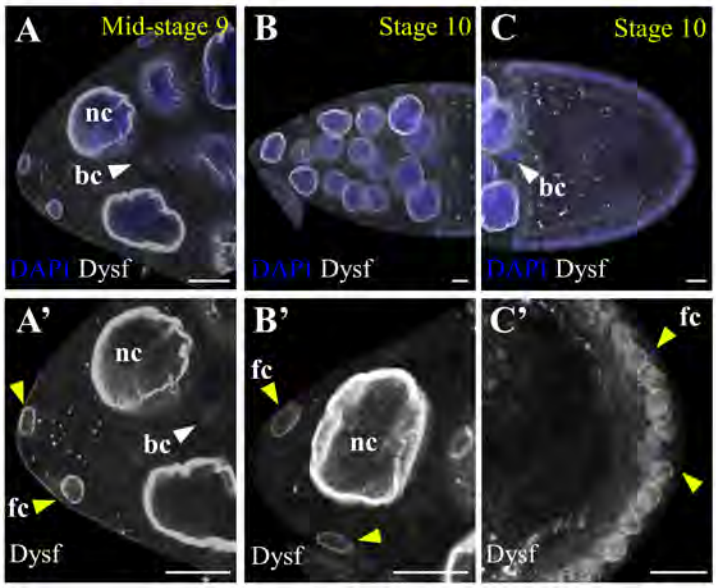
A
Mid-stage 9
nc
bc
DAPI Dysf
B
Stage 10
DAPI Dysf
C
Stage 10
bc
DAPI Dysf
A'
nc
bc
fc
Dysf
B'
fc
nc
Dysf
C'
fc
Dysf

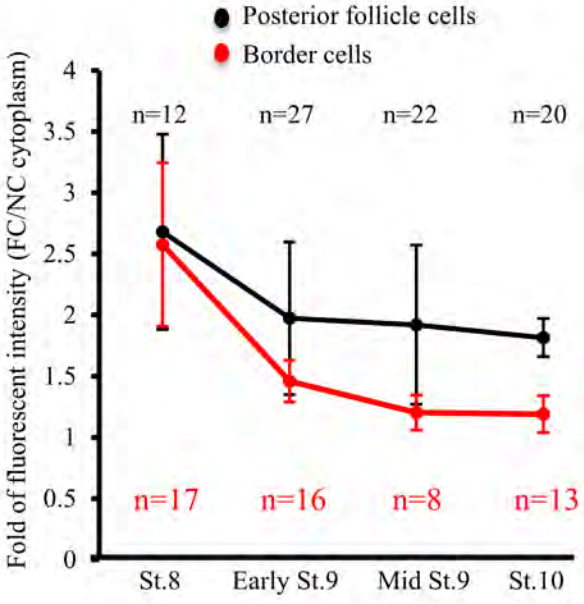
D
Posterior follicle cells
Border cells
Fold of fluorescent intensity (FC/NC cytoplasm)
n=12
n=27
n=22
n=20
n=17
n=16
n=8
n=13
St.8
Early St.9
Mid St.9
St.10

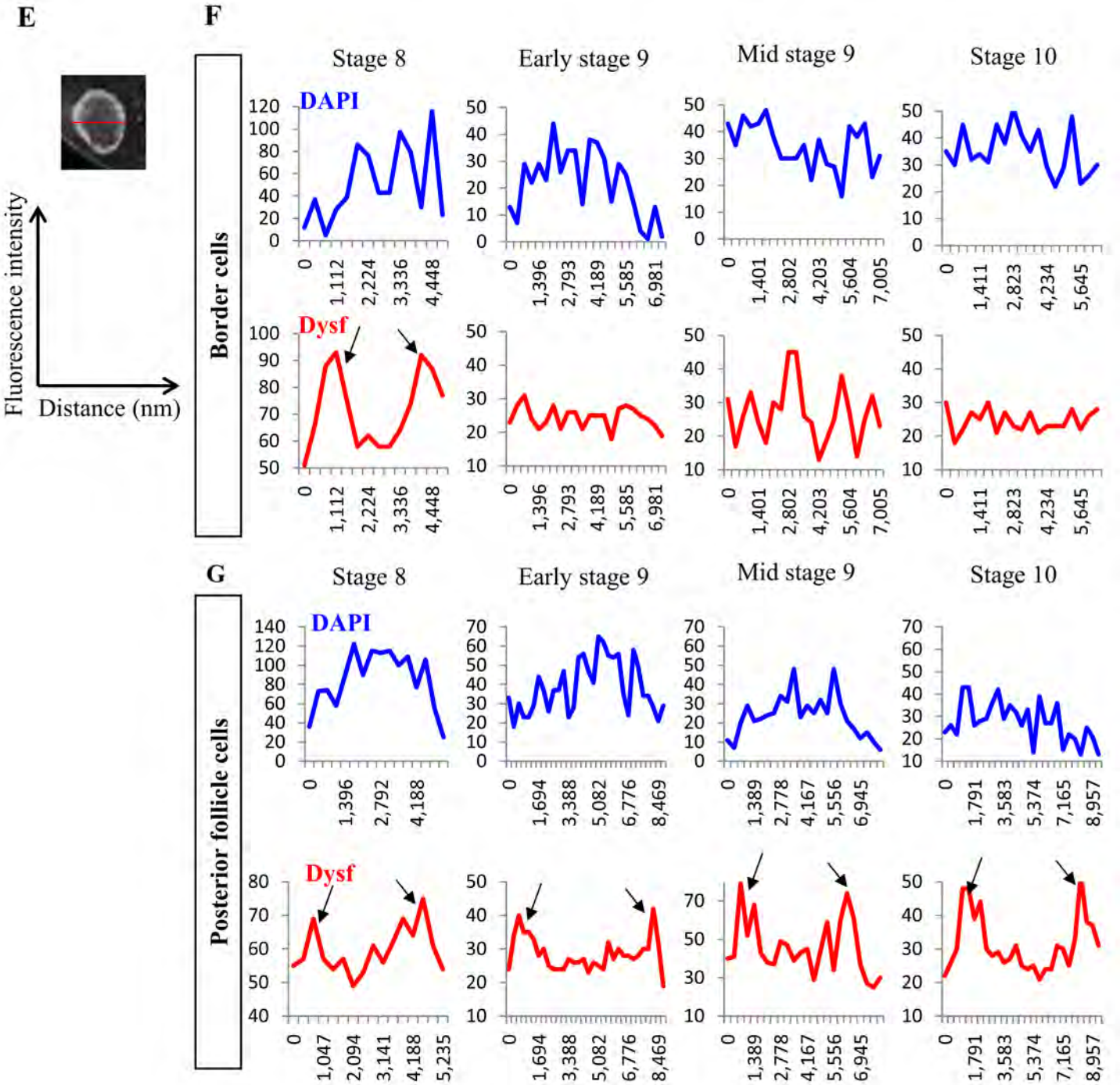
E
F
G
Fluorescence intensity
Distance (nm)
Border cells
Posterior follicle cells
Stage 8
Early stage 9
Mid stage 9
Stage 10
DAPI
Dysf

Fig. S6: Spatiotemporal downregulation of Dysf protein during border cell migration. (**A** to **C**) Confocal micrographs of egg chambers stained with anti-Dysf antibody demonstrate Dysf expression in nurse cells (nc), follicle cells (fc; yellow arrowhead) and border cells (bc; white arrowhead), which are magnified below. DAPI labels the nucleus (blue). (**D**) Quantification of Dysf expression in border cells and posterior follicles at different stages of egg chambers. Fold change of Dysf staining was determined by the fluorescence intensity of border cells (red plot) and posterior follicle cells (black plot) divided by the background of nurse cell cytoplasm. n represents the number of border cells or follicle cells examined. Error bars indicate SD. (**E**) Illustration of fluorescence intensity profiling. The fluorescence intensity was measured along the center of the nucleus (red line in upper panel) and plotted as distance versus intensity (lower panel). (**F** to **G**) Dysf fluorescence intensity profiles of border cells (F) and posterior follicles (G). DAPI plots serve as a control. Error bars indicate SD. Scale bar: 20 μm.

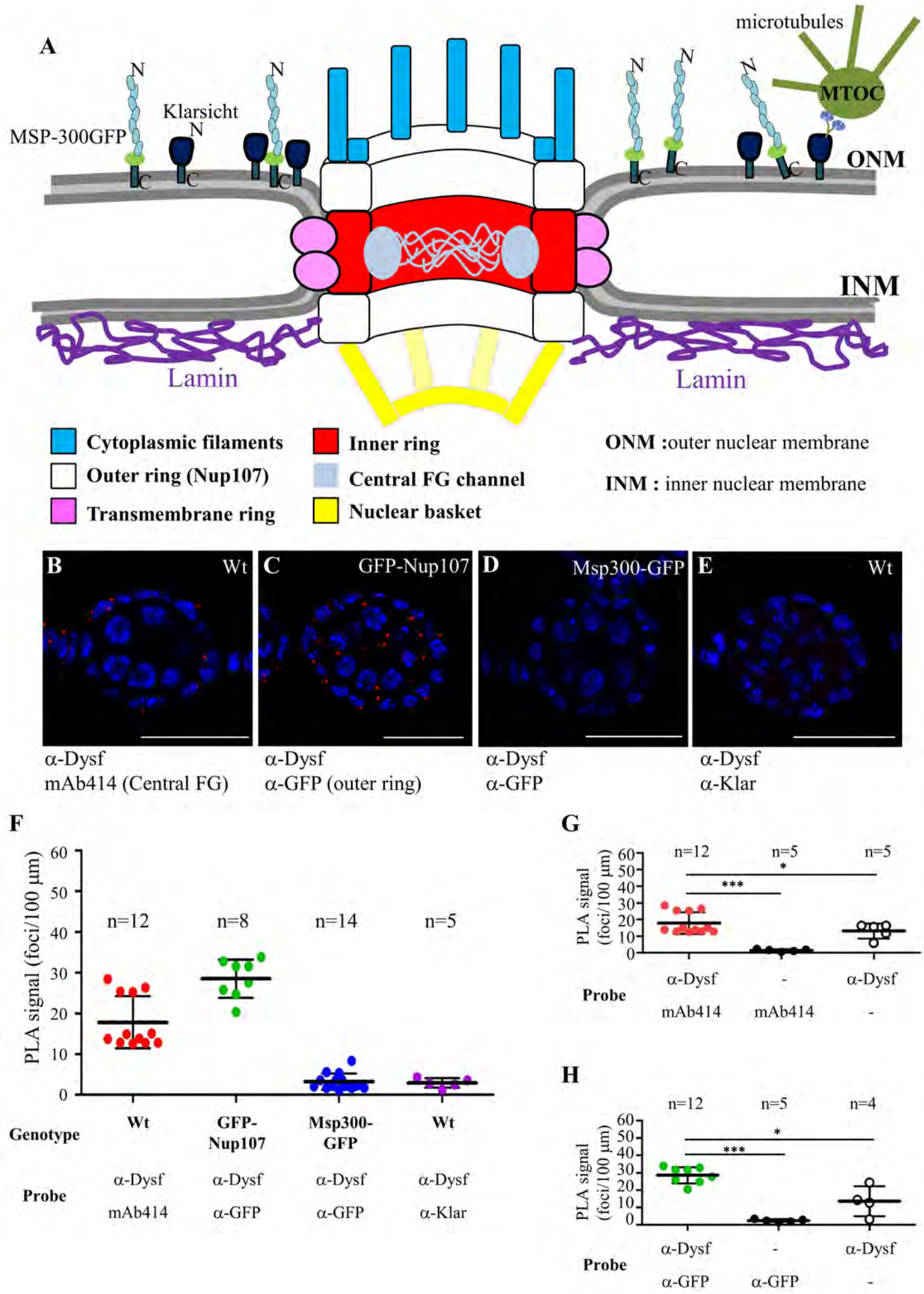
A
microtubules
MTOC
MSP-300GFP
Klarsicht
N
C
ONM
INM
Lamin
Lamin
Cytoplasmic filaments
Outer ring (Nup107)
Transmembrane ring
Inner ring
Central FG channel
Nuclear basket
ONM :outer nuclear membrane
INM : inner nuclear membrane
B Wt
C GFP-Nup107
D Msp300-GFP
E Wt
α-Dysf
mAb414 (Central FG)
α-Dysf
α-GFP (outer ring)
α-Dysf
α-GFP
α-Dysf
α-Klar
F
PLA signal (foci/100 µm)
n=12
n=8
n=14
n=5
Genotype
Wt
GFP-Nup107
Msp300-GFP
Wt
Probe
α-Dysf mAb414
α-Dysf α-GFP
α-Dysf α-GFP
α-Dysf α-Klar
G
n=12
n=5
n=5
*
***
PLA signal (foci/100 µm)
Probe
α-Dysf mAb414
- mAb414
α-Dysf -
H
n=12
n=5
n=4
*
***
PLA signal (foci/100 µm)
Probe
α-Dysf α-GFP
- α-GFP
α-Dysf -

Fig. S7: Interaction of Dysf with components of the nuclear pore complex. (**A**) Schematic of the nuclear pore complex and associated nuclear membrane structure. To pinpoint Dysf localization on the nuclear envelope, distinct markers were employed for *in situ* PLA assay using anti-Dysf antibodies, including Msp300, Klarsicht, Nup107 and the central FG channel. (**B** to **E**) Confocal images of egg chambers stained with DAPI (blue) reveal PLA interactions (red) with indicated antibody probes. Red speckles indicate that Dysf physically interacts with FG-rich-repeat domain Nups (B) and Nup107 (C), but not outer nuclear membrane proteins (D and E). mAB414 antibody recognizes the FG repeat sequence in channel nucleoporins, such as Nup62. (**F** to **H**) Quantitative analyses of protein-protein interactions by PLA. n indicates the total number of egg chambers scrutinized; *$p < 0.05$, **$p < 0.01$, two-tailed t test. Error bars indicate SD. Scale bars: 20 μm.

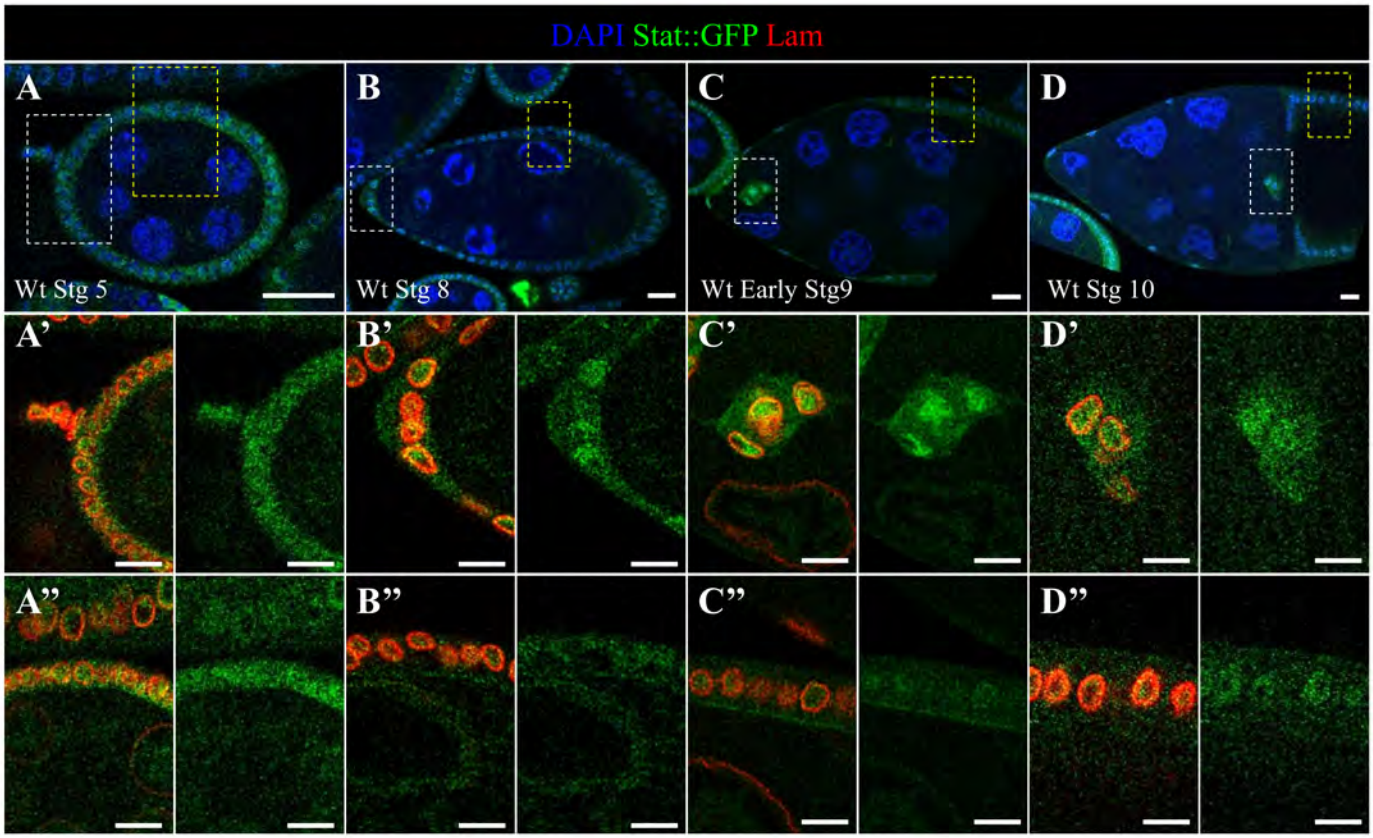
DAPI Stat::GFP Lam
A
B
C
D
Wt Stg 5
Wt Stg 8
Wt Early Stg9
Wt Stg 10
A'
B'
C'
D'
A"
B"
C"
D"

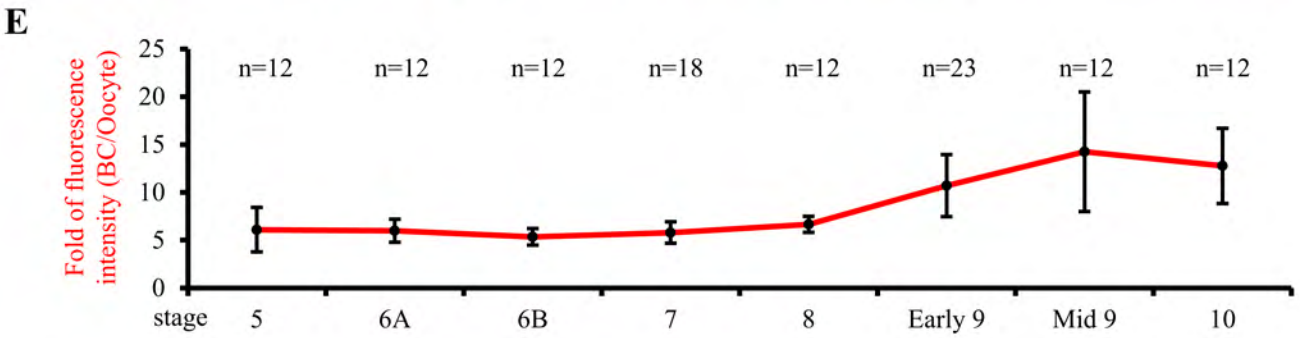
E
Fold of fluorescence intensity (BC/Oocyte)
25
20
15
10
5
0
n=12
n=12
n=12
n=18
n=12
n=23
n=12
n=12
stage
5
6A
6B
7
8
Early 9
Mid 9
10

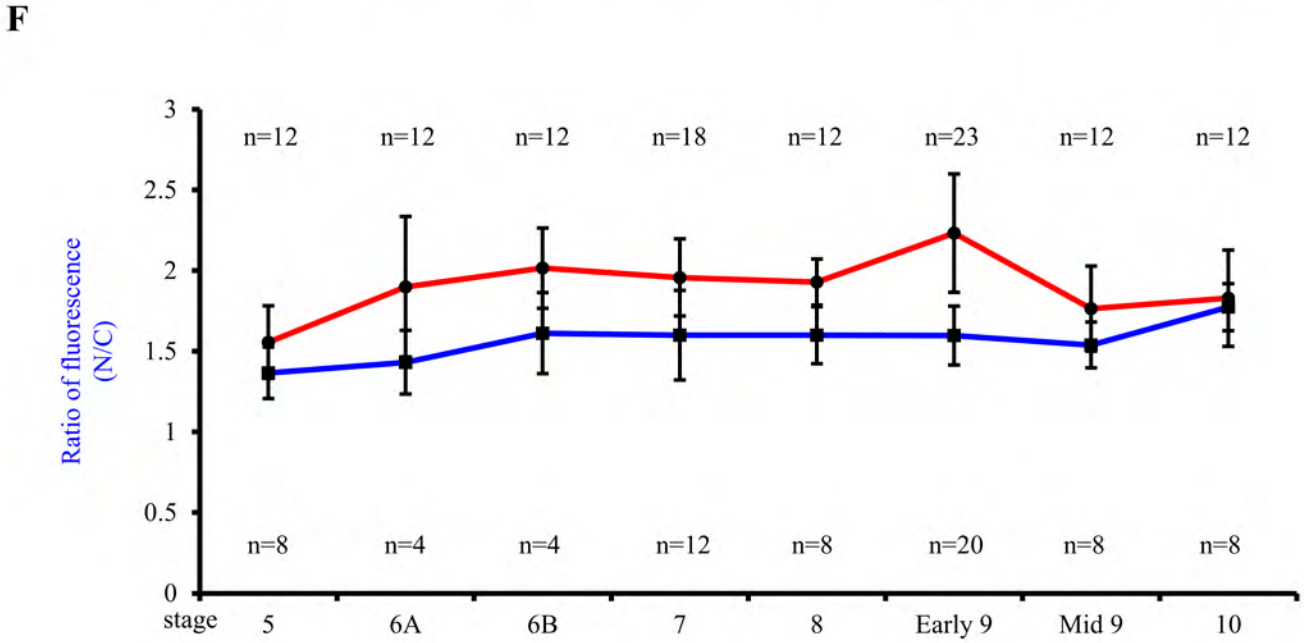
F
Ratio of fluorescence (N/C)
3
2.5
2
1.5
1
0.5
0
n=12
n=12
n=12
n=18
n=12
n=23
n=12
n=12
n=8
n=4
n=4
n=12
n=8
n=20
n=8
n=8
stage
5
6A
6B
7
8
Early 9
Mid 9
10

Fig. S8: Subcellular distribution of Stat::GFP in *Drosophila* oogenesis. (**A** to **D**) Confocal micrographs of egg chambers demonstrate Stat::GFP expression pattern (green), and lower panels show enlargements of anterior follicle cells or border cells (white-dotted boxes) and dorsal/ventral follicles (yellow-dotted boxes). DAPI (blue) and anti-Lamin (red) staining label the nuclei. (**E**) The fold change and (**F**) the N/C ratio of Stat::GFP signal in anterior follicle cells (stage 5 to 8) and border cells (stage 9 to 10) are depicted by the red plots. The blue plot represents the Stat::GFP N/C ratio of dorsal/ventral follicle cells at different stages. n indicates the number of border cells examined. Error bars indicate SD. Scale bar: Scale bar: 20 μm (A to D) and 10 μm (A'-A'' to D'-D'')

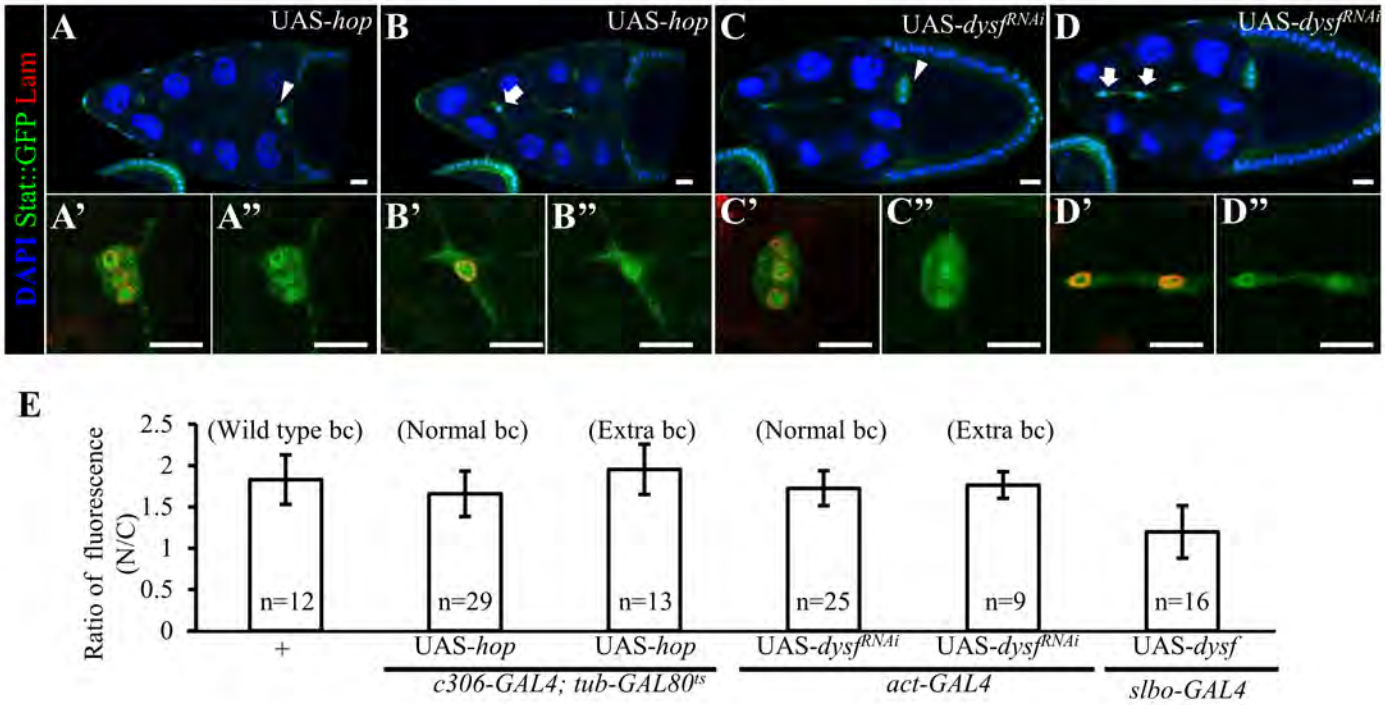

Fig. S9: Quantitative analysis of the N/C ratio of Stat::GFP in ectopic border cells. (**A** to **D**) Different focal planes of micrographs taken from the same egg chambers display extra recruited border cells (Extra bc; arrows) and normally migrating border cells that reach the oocyte (Normal bc; arrowheads) in the indicated genotypes. (**E**) Quantitation results of the N/C ratio of Stat::GFP in border cells. Stage-10 egg chambers were employed for analysis. n represents the number of border cells examined. Error bars indicate SD. Scale bar: 20 μm in A to D; 10 μm in A', A" to D' and D".

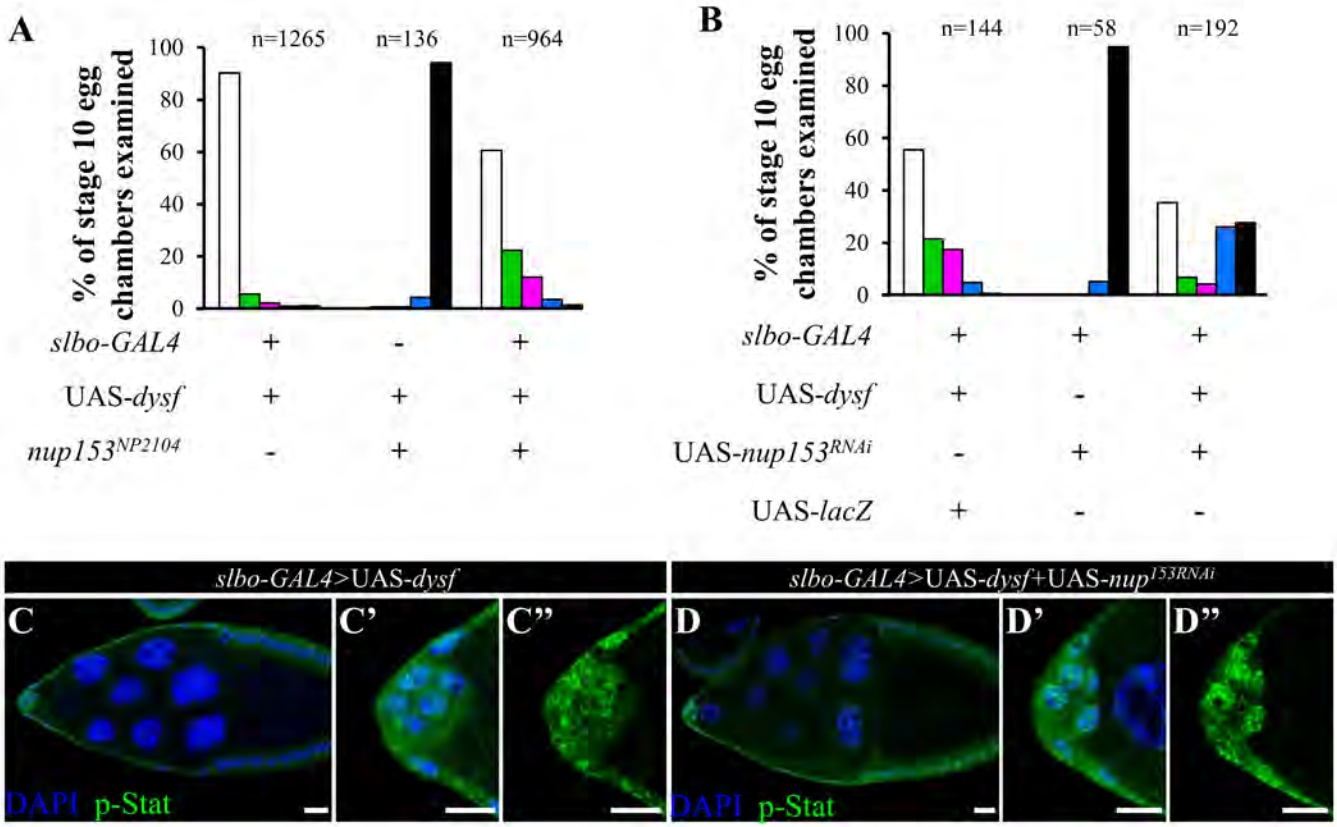

Fig. S10: Genetic interaction of *nup153* with *dysf* contributes to border cell migration and Stat nuclear import. (**A** and **B**) Insertion of the *nup153*^{NP2104} transposon and RNAi knockdown of *nup153* rescues the border cell migration defect caused by Dysf overexpression. Quantitation of border cell migration for the indicated genotypes. (**C** and **D**) Egg chambers stained with anti-p-Stat antibodies reveal that expression of *nup153* double-stranded RNA restores nuclear accumulation of p-Stat (green) in border cells overexpressing Dysf (D) relative to the control (C). DAPI stains nuclei (blue). n indicates the total number of egg chambers examined. Scale bar: 20 μm.

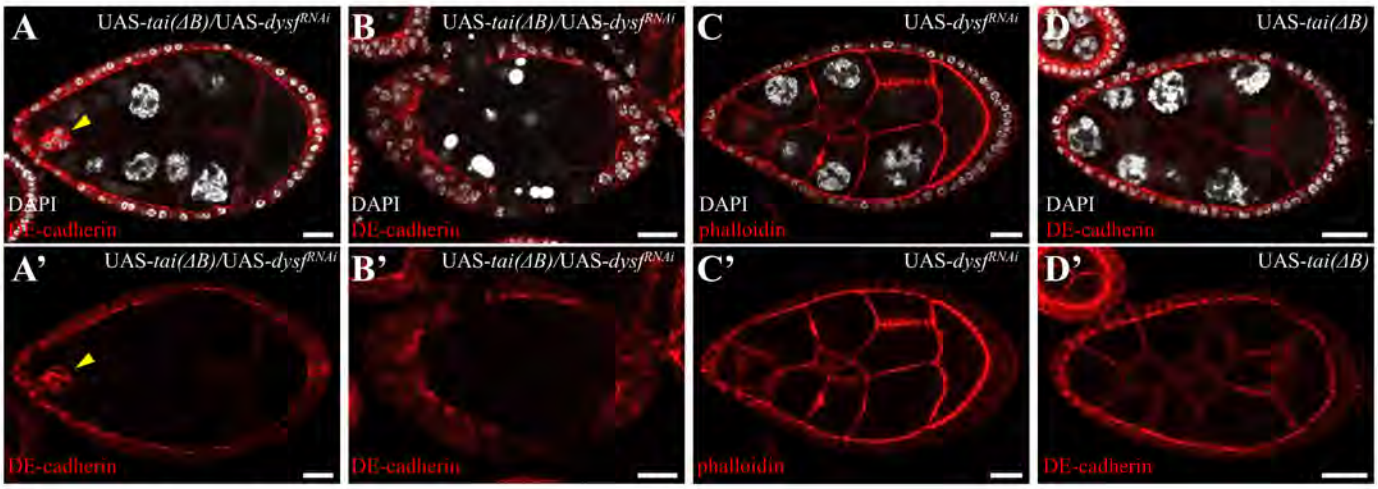

E **Stage 8 egg chamber**

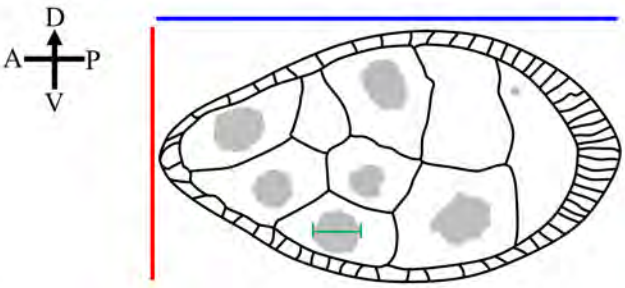

$$\text{Aspect ratio} = \frac{\text{A-P length}}{\text{D-V width}} = 1.91 \pm 0.07 \text{ s.d.}$$

Nurse cell nuclear diameter (μm) = 23.64 ± 1.66 s.d.

F

genotypes	number of stg. 8 egg chambers with early migration	number of ovariole with stg. 8 egg chamber
UAS-*dysf*^{RNAi}/UAS-*tai(ΔB)*	5	48
UAS-*dysf*^{RNAi}	0	25
UAS-*tai(ΔB)*	0	17

Fig. S11: Co-expression of *dysf*^{RNAi} and *Tai (ΔB)* induced precocious migration in border cells. Confocal images of egg chambers stained with DAPI (white) to mark nuclei and with anti-DE-cadherin (**A**, **B** and **D**, red) and phalloidin (**C**, red) to make cell margins. Transgenes were expressed by *actin-GAL4* in all follicle cells. (**A**) A stage 8 egg chamber displays early detachment and migration of border cells (arrowheads) caused by *dysf*^{RNAi}*-Tai (ΔB)* co-expression. (**B**) Co-expression of *dysf*^{RNAi} and *Tai (ΔB)* caused egg chamber degeneration. (**C** and **D**) Overexpression of UAS-*tai(ΔB)* or UAS-*dysf*^{RNAi} alone showed normal development in stage 8 egg chambers. (**E**) Illustration showing the definition of stage 8 egg chamber by the aspect ration and the nucleus size of nurse cells. An aspect ration is the ratio of the anterior-posterior length to the dorsal-ventral width of an egg chamber. (**F**) Quantification of stage 8 egg chambers with the precocious migration phenotype. Scale bar: 20 μm.

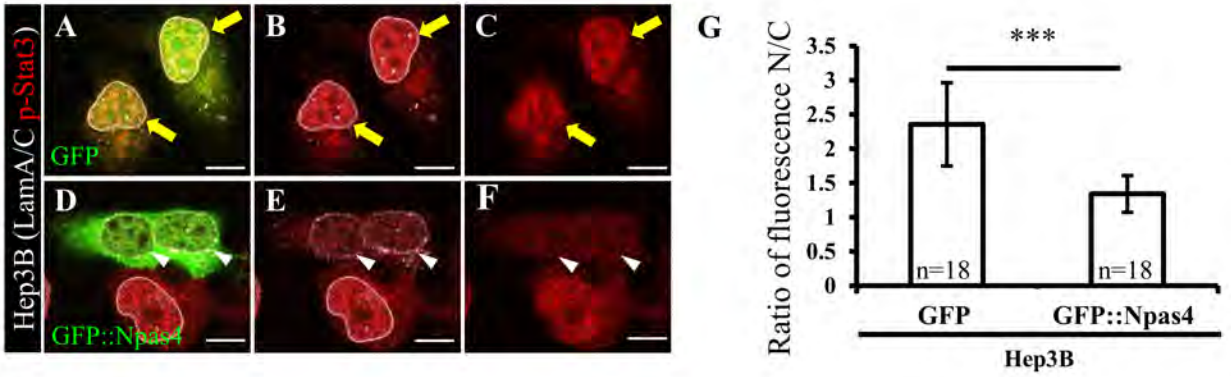

Fig. S12: Overexpression of Npas4 inhibits the nuclear localization of phospho-Stat3 in cancer cells. (**A** to **F**) Confocal images of Hep3B cells stained with anti-p-Stat3 (red) and anti-Lamin A/C antibody (white). (**A** to **C**) IL-6 treatment induces p-Stat3 accumulation in the nuclei of control cells visualized by GFP (yellow arrows; green). (**D** to **F**) Transfection of GFP::Npas4 (green) diminished the nuclear distribution of p-Stat3 (white arrowheads). (**G**) Quantification of the N/C ratio of anti-p-Stat3 staining. n means the inspected sample size; *P<0.001, two-tailed t test. n indicates the number of cells examined. Error bars indicate SD. Scale bars: 10 μm

Table S1. List of fly genotypes

Figure	Genotype
Fig. 1	
Fig. 1A-B	*Stat92E-GFP*
Fig. 1C	*slbo-GAL4,* UAS-*nls-gfp*; UAS-*lacZ*
Fig. 1D	*slbo-GAL4,* UAS-*nls-gfp*/UAS-*dysf*
Fig. 1E	*slbo-GAL4,* UAS-*nls-gfp*;UAS-*lacZ* *slbo-GAL4,* UAS-*nls-gfp*/UAS-*dysf*
Fig. 1F	*slbo-GAL4; Stat92E-GFP*/UAS-*lacZ*
Fig. 1G	*slbo-GAL4,* UAS-*mCD8-gfp*; UAS-*lacZ*
Fig. 1H	*slbo-GAL4*/UAS-*dysf; Stat92E-GFP*
Fig. 1I-J	*slbo-GAL4,* UAS-*mCD8-gfp*/UAS-*dysf*
Fig. 1K	*slbo-GAL4,* UAS-*mCD8-gfp*;UAS-*lacZ* *slbo-GAL4,* UAS-*mCD8-gfp*/UAS-*dysf*
Fig. 1L-M	w^{1118}
Fig. 1N	*slbo-GAL4*/UAS-*dysf*
Fig. 2	
Fig. 2A	*c306-GAL4;* UAS-*upd; tub-GAL80^{ts}*/UAS-*lacZ*
Fig. 2B	*c306-GAL4;* UAS-*hop; tub-GAL80^{ts}*/UAS-*lacZ*
Fig. 2C	*c306-GAL4;* UAS-*lacZ; tub-GAL80^{ts}*/UAS-*dysf-3xHA*
Fig. 2D	*c306-GAL4;* UAS-*upd; tub-GAL80^{ts}*/UAS-*dysf-3xHA*
Fig. 2E	*c306-GAL4;* UAS-*hop; tub-GAL80^{ts}*/UAS-*dysf-3xHA*
Fig. 2F	*c306-GAL4;* UAS-*lacZ; tub-GAL80^{ts}*/UAS-*lacZ*
Fig. 2G	*c306-GAL4;* UAS-*lacZ; tub-GAL80^{ts}*/UAS-*lacZ* *c306-GAL4;* UAS-*lacZ; tub-GAL80^{ts}*/UAS-*dysf-3xHA* *c306-GAL4;* UAS-*hop; tub-GAL80^{ts}*/UAS-*lacZ* *c306-GAL4;* UAS-*upd; tub-GAL80^{ts}*/UAS-*lacZ* *c306-GAL4;* UAS-*hop; tub-GAL80^{ts}*/UAS-*dysf-3xHA* *c306-GAL4;* UAS-*upd; tub-GAL80^{ts}*/UAS-*dysf-3xHA*

Figure	Genotype
Fig. 3	
Fig. 3A-C	*hsFLP*; *Stat92E-GFP*; FRT82B, *ubi-rfp*/FRT82B
Fig. 3D-F	*hsFLP*; *Stat92E-GFP*; FRT82B, *ubi-rfp*/FRT82B, $dysf^{2}$
Fig. 3G	*hsFLP*; *Stat92E-GFP*; FRT82B, *ubi-rfp*/FRT82B *hsFLP*; *Stat92E-GFP*; FRT82B, *ubi-rfp*/FRT82B, $dysf^{2}$
Fig. 3H	w^{1118}
Fig. 3I	$dysf^{2/3}$
Fig. 3J	$dysf^{2}/+$ $dysf^{3}/+$ $dysf^{2/3}$
Fig. 3K	*act-GAL4*/UAS-$dysf^{RNAi}$
Fig. 3L	*act-GAL4* *act-GAL4*/UAS-$dysf^{RNAi}$
Fig. 3M-P	*hsFLP*;; FRT82B, *ubi-rfp*/FRT82B, $dysf^{JW}$
Fig. 4	
Fig. 4A-F	*slbo-GAL4,* UAS-*nls-gfp*
Fig. 4G-H	*slbo-GAL4;* UAS-*lamin::gfp*
Fig. 4J-N	w^{1118}
Fig. 5	
Fig. 5A-B	*slbo-GAL4/stat92e-stat92e::gfp*
Fig. 5C	*slbo-GAL4/stat92e-stat92e::gfp*, UAS-*dysf*
Fig. 5D	*stat92e-stat92e::gfp*
Fig. 5E	*stat92e-stat92e::gfp,* UAS-*dysf*; *24B-GAL4*
Fig. 5F	*stat92e-stat92e::gfp*
Fig. 5G	*stat92e-stat92e::gfp,* UAS-*dysf* ; *24B-GAL4*
Fig. 5H	*24B-GAL4*/UAS-*lacZ*
Fig. 5I	UAS-*dysf*; *24B-GAL4*
Fig. 5J	*stat92e-stat92e::gfp* *stat92e-stat92e::gfp,* UAS-*dysf*; *24B-GAL4*
Fig. 5K	*24B-GAL4*/UAS-*lacZ* UAS-*dysf*; *24B-GAL4*

Figure	Genotype
Fig. 6	
Fig. 6A	*N-APEX2-dysf*
Fig. 6B	*slbo-GAL4;* UAS-*dysf-3xHA, tub-GAL80^{ts}*
Fig. 6C	*24B-GAL4*/UAS-*dysf-3xHA*
Fig. 6D	*act-GAL4; tub-GAL80^{ts}*/UAS-*dysf-3xHA*
Fig. 6E	*act-GAL4; tub-GAL80^{ts}*/UAS-*dysf-3xHA* *stat92e-stat92e::gfp*
Fig. 6F	*slbo-GAL4,* UAS-*nls-gfp;* UAS-*dysf-3xHA, tub-GAL80^{ts}*/UAS-*lacZ* *slbo-GAL4,* UAS-*nls-gfp*/UAS-*pen;* UAS-*dysf-3xHA, tub-GAL80^{ts}* *slbo-GAL4,* UAS-*nls-gfp*/UAS-*pen; tub-GAL80^{ts}*/UAS-*lacZ*
Fig. 6G	*slbo-GAL4,* UAS-*nls-gfp;* UAS-*dysf-3xHA, tub-GAL80^{ts}*/UAS-*lacZ*
Fig. 6H	*slbo-GAL4,* UAS-*nls-gfp*/UAS-*pen;* UAS-*dysf-3xHA, tub-GAL80^{ts}*

Figure	Genotype
Fig. S1	
Fig. S1B-H	*hsFLP;* UAS-*dysf; AyGAL4*, UAS-*rfp/Stat92E-GFP*
Fig. S1I-J	*hsFLP;* UAS-*dysf; AyGAL4*, UAS-*rfp/Stat92E-GFP* *hsFLP;* UAS-*lacZ; AyGAL4*, UAS-*rfp/Stat92E-GFP*
Fig. S2	
Fig. S2A-E	*slbo-GAL4,* UAS-*nls-gfp*
Fig. S2F-G	*slbo-GAL4,* UAS-*nls-gfp*/UAS-*dysf* *slbo-GAL4,* UAS-*nls-gfp;* UAS-*lacZ*
Fig. S2H-I	*c306-GAL4;* UAS-*hop; tub-GAL80^{ts}*
Fig. S2J-K	*act-GAL4, tub-GAL80^{ts};* UAS-*dysf^{RNAi}*
Fig. S2L	*c306-GAL4;; tub-GAL80^{ts}*/UAS-*lacZ* *c306-GAL4;* UAS-*hop; tub-GAL80^{ts}*
Fig. S2M	*act-GAL4, tub-GAL80^{ts};* UAS-*lacZ* *act-GAL4, tub-GAL80^{ts};* UAS-*dysf^{RNAi}*
Fig. S2N	*slbo-GAL4,* UAS-*nls-gfp;*UAS-*dysf-3xHA, tub-GAL80^{ts}*/UAS-*lacZ* *slbo-GAL4,* UAS-*nls-gfp*/UAS-*pen;* UAS-*dysf-3xHA, tub-GAL80^{ts}* *slbo-GAL4,* UAS-*nls-gfp*/UAS-*pen; tub-GAL80^{ts}*/UAS-*lacZ*
Fig. S3	
Fig. S3A-B	*stat-lacZ*
Fig. S3C-D	*slbo-GAL4,* UAS-*nls-gfp;* UAS-*dysf-3xHA, tub-GAL80^{ts}/stat-lacZ*
Fig. S3E	*stat-lacZ* *slbo-GAL4,* UAS-*nls-gfp;* UAS-*dysf-3xHA, tub-GAL80^{ts}/stat-lacZ*
Fig. S4	
Fig. S4A-B	*hsFLP*; *Stat92E-GFP*; FRT82B, *ubi-rfp*/FRT82B, *dysf^{2}*
Fig. S4C-D	*hsFLP*; FRT82B, *ubi-gfp*/FRT82B, *dysf^{2}*
Fig. S4E	*hsFLP*; FRT82B, *ubi-rfp*/FRT82B, *dysf^{2}*
Fig. S5	
Fig. S5B-D	*hsFLP*; FRT82B, *ubi-gfp*/FRT82B, *dysf^{2}*
Fig. S6	
Fig. S6A-G	*slbo-GAL4,* UAS-*nls-gfp*

Figure	Genotype
Fig. S7	
Fig. S7B	*w*^{1118}
Fig. S7C	*gfp-nup107*
Fig. S7D	*msp300-gfp*
Fig. S7E	*w*^{1118}
Fig. S7F	*w*^{1118} *gfp-nup107* *msp300-gfp*
Fig. S7G	*w*^{1118}
Fig. S7H	*gfp-nup107*
Fig. S8	
Fig. S8A-F	*stat92e-stat92e::gfp*
Fig. S9	
Fig. S9A-B	*c306-GAL4;* UAS-*hop/stat92e-stat92e::gfp; tub-GAL80*^{ts}
Fig. S9C-D	*act-GAL4, tub-GAL80*^{ts}*/stat92e-stat92e::gfp;* UAS-*dysf*^{RNAi}
Fig. S9E	*stat92e-stat92e::gfp* *c306-GAL4;* UAS-*hop/stat92e-stat92e::gfp; tub-GAL80*^{ts} *act-GAL4, tub-GAL80*^{ts}*/stat92e-stat92e::gfp;* UAS-*dysf*^{RNAi} *slbo-GAL4/stat92e-stat92e::gfp*, UAS-*dysf*
Fig. S10	
Fig. S10A	*slbo-GAL4,* UAS-*nls-gfp;* UAS-*dysf-3xHA, tub-GAL80*^{ts} *nup153*^{NP2104};UAS-*dysf-3xHA, tub-GAL80*^{ts} *nup153*^{NP2104}*; slbo-GAL4,* UAS-*nls-gfp;* UAS-*dysf-3xHA, tub-GAL80*^{ts}
Fig. S10B	*slbo-GAL4,* UAS-*nls-gfp;* UAS-*dysf-3xHA, tub-GAL80*^{ts}/UAS-*lacZ* *slbo-GAL4,* UAS-*nls-gfp*/UAS-*nup153*^{RNAi} *slbo-GAL4,* UAS-*nls-gfp*/UAS-*nup153*^{RNAi}*;* UAS-*dysf-3xHA, tub-GAL80*^{ts}
Fig. S10C	*slbo-GAL4,* UAS-*nls-gfp;* UAS-*dysf-3xHA, tub-GAL80*^{ts}/UAS-*lacZ*
Fig. S10D	*slbo-GAL4,* UAS-*nls-gfp*/UAS-*nup153*^{RNAi}*;* UAS-*dysf-3xHA, tub-GAL80*^{ts}
Fig. S11	
Fig. S11A-B	*act-GAL4, tub-GAL80*^{ts}*;* UAS-*tai(ΔB)*/UAS-*dysf*^{RNAi}
Fig. S11C	*act-GAL4, tub-GAL80*^{ts}*;* UAS-*dysf*^{RNAi}
Fig. S11D	*act-GAL4, tub-GAL80*^{ts}*;* UAS-*tai(ΔB)*
Fig. S11E	*act-GAL4, tub-GAL80*^{ts}*;* UAS-*tai(ΔB)*/UAS-*dysf*^{RNAi} *act-GAL4, tub-GAL80*^{ts}*;* UAS-*dysf*^{RNAi} *act-GAL4, tub-GAL80*^{ts}*;* UAS-*tai(ΔB)*